Electronic Supplementary Material (ESI) for Dalton Transactions.

Supplementary Information

Near-infrared photothermal performance of a metal organic framework-based composite

Jing Sun, Kuan Pang, Tian-Fu Liu, Jibin Song and Rong Cao

1. Materials and charaterization

1.1 Materials

Poly(vinylpyrrolidone) (PVP), sodium selenite (Na_2SeO_3), bismuth nitrate pentahydrate ($Bi(NO_3)_3 \cdot 5H_2O$), zinc nitrate hexahydrate ($Zn(NO_3)_2 \cdot 6H_2O$), 2-methylimidazole (2-MIM), deionized water (DI), ethylene glycol (EG), methanol (MeOH), acetone, ethanol (EtOH), methyl cyanide (MeCN), hydrazine hydrate. Unless otherwise mentioned, all reagents and solvents were purchased from commercial sources and used as received without further purification.

1.2 Characterization

PXRD was performed on Rikagu Miniflex 600 Benchtop X-ray diffraction instrument. TGA was performed on a Seiko S-II instrument, and the dried crystalline samples were heated at a rate of 5 ºC/min up to 800 ºC and then cooled to room temperature under N_2 atmosphere. The N_2 isotherms of the samples were measured using ASAP 2460 from Micromeritics Co. Ltd. SEM was performed on a JSM6700-F Field Emission scanning electron microscope. TEM was performed on a Tecnai F20 Field transmission scanning electron microscope. UV-Vis absorbance of liquid samples were collected at room temperature on a PerkinElmer Lambda 365 spectrophotometer equipped with Labsphere integrating over the spectral range λ = 500- 900 nm, and the solid samples were collected at room temperature on a Perkin Elmer Lambda 950 spectrophotometer equipped with Labsphere integrating over the spectral range λ = 300-850 nm using $BaSO_4$ as standards.

2. Scanning electron microscopy (SEM)

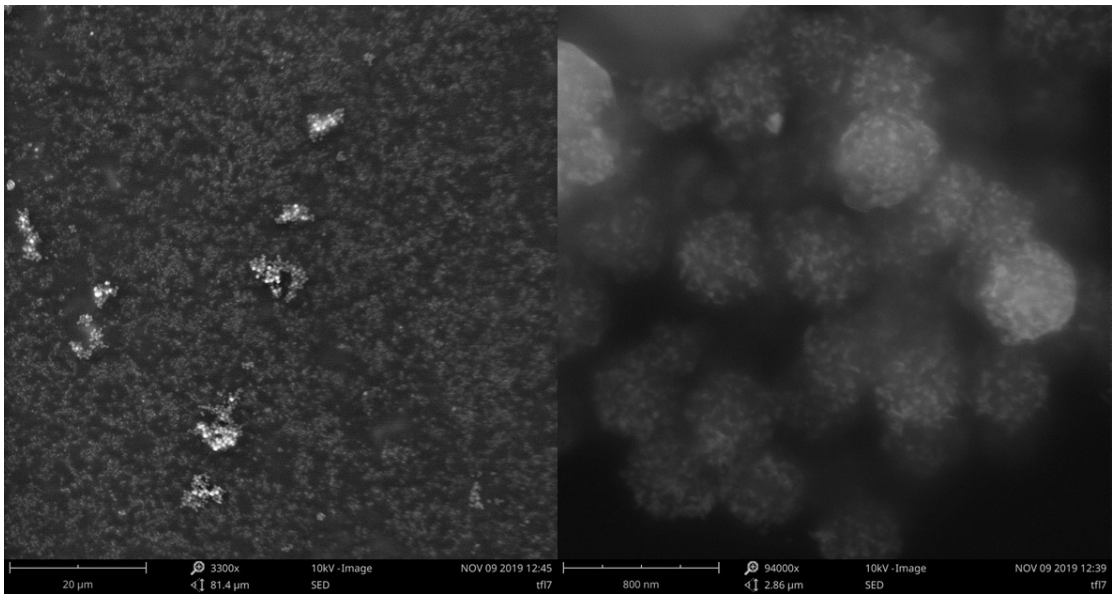

Figure S1. SEM images of Bi_2Se_3@ZIF-8 NPs.

3. Transmission scanning electron microscopy

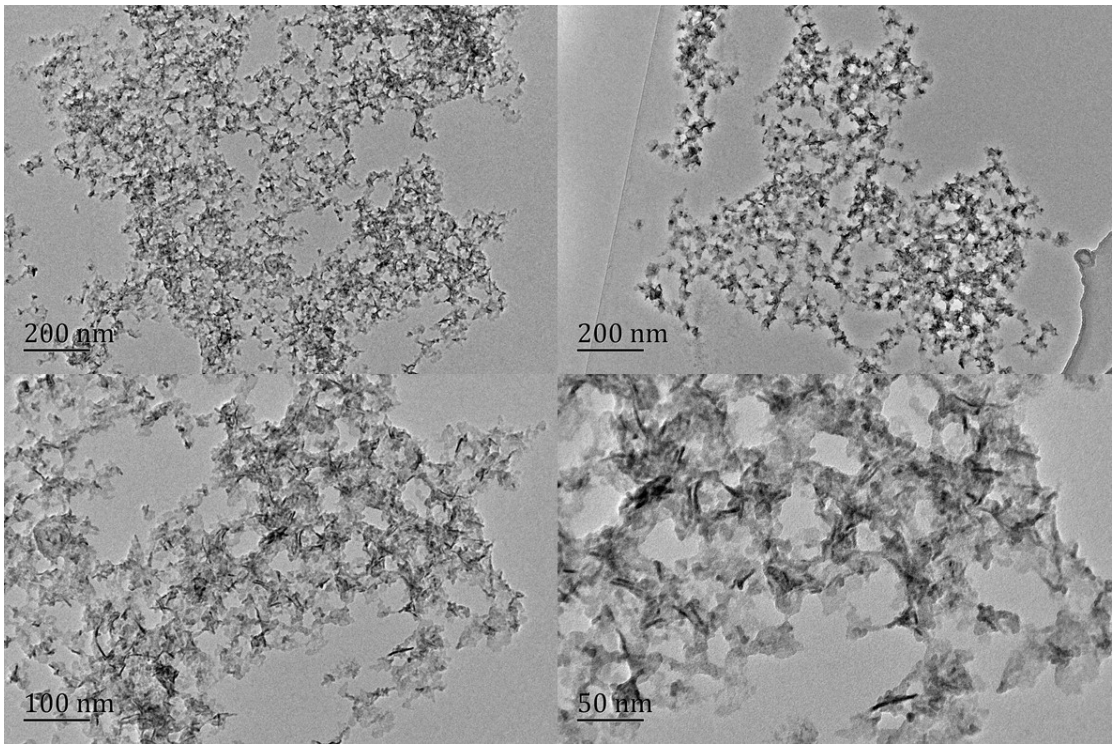

Figure S2. TEM images of Bi_2Se_3 NPs.

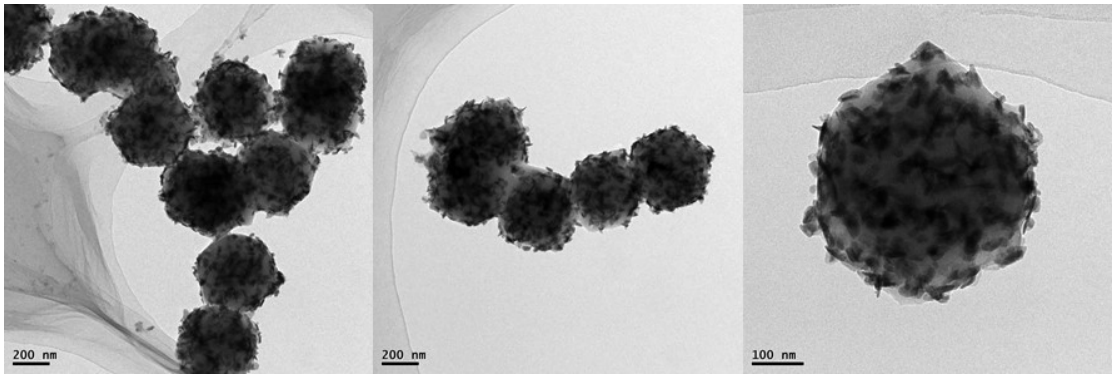

Figure S3. TEM images of Bi_2Se_3@ZIF-8 NPs.

4. Powder X-ray diffraction patterns

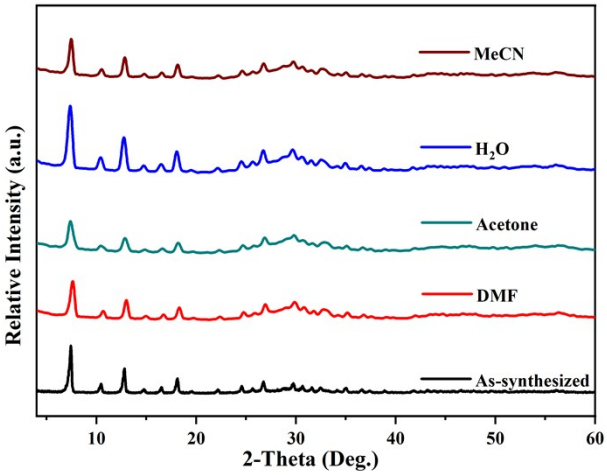

Figure S4. PXRD patterns of Bi_2Se_3@ZIF-8 NPs exposed to different solvent after 24 h.

5. IR spectra

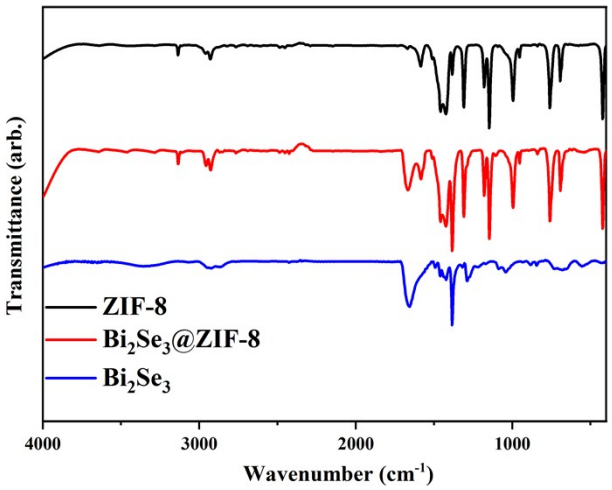

Figure S5. IR spectra of Bi_2Se_3 NPs (blue), ZIF-8 (black) and Bi_2Se_3@ZIF-8 NPs (red).

6. Pore size distribution

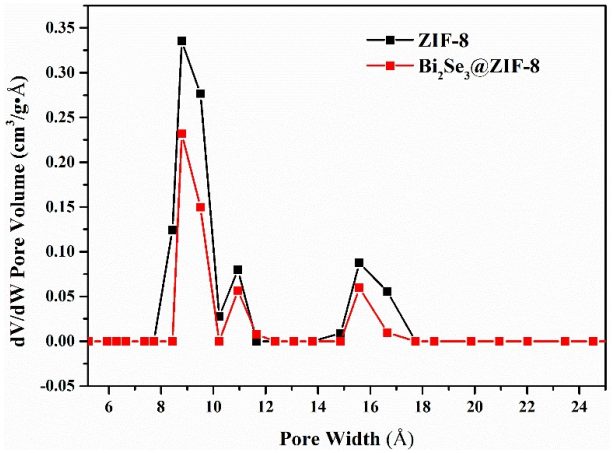

Figure S6. Pore size distribution of ZIF-8 (black) and Bi_2Se_3@ZIF-8 (red).

7. Thermogravimetric analyses (TGA)

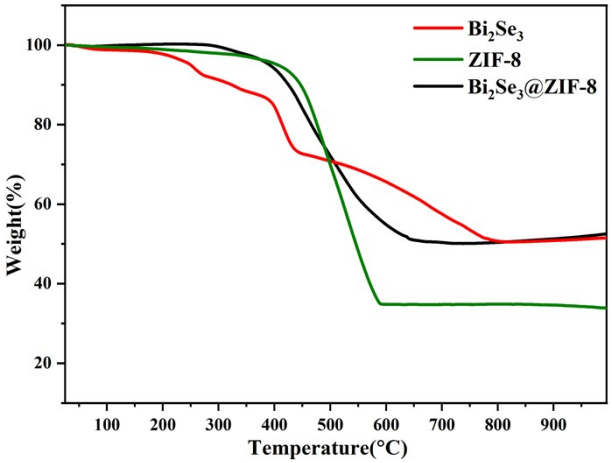

Figure S7. TGA curves of Bi_2Se_3 NPs (red), ZIF-8 (green) and Bi_2Se_3@ZIF-8 NPs (black).

8. Ultraviolet-visible-near infrared absorption spectra

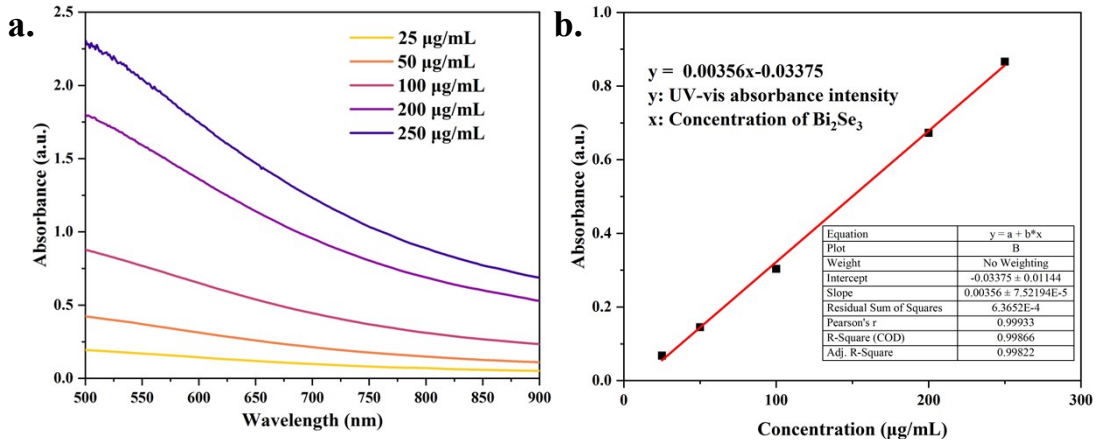

Figure S8. (a) Absorbance spectra of the Bi_2Se_3 NPs dispersed in water at concentrations of 25, 50, 100, 200, 250 μg/mL. (b) Absorbance intensity for λ = 808 nm at different concentrations of Bi_2Se_3 NPs.

9. Transient photocurrent responses

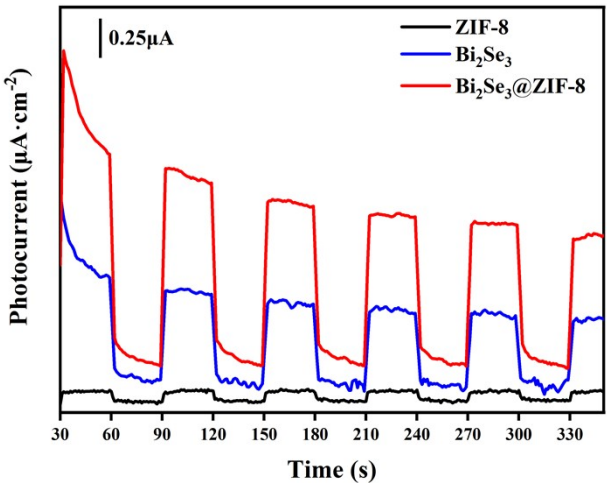

Figure S9. Transient photocurrent responses of ZIF-8, Bi_2Se_3, and Bi_2Se_3@ZIF-8.

10. Photothermal experiments

The accurate photothermal conversion efficiency (PTCE, η) of Bi_2Se_3@ZIF-8 was calculated according to a previously described method. In general, the powdery sample was suspended into 1 mL MeOH (0.7 mg/mL) at room temperature (30 ºC). The mixture was irradiated for 10 minutes (808 nm, 3 $W \cdot cm^{-2}$). Then the laser was shut off to allow the system to cool down to room temperature naturally. Both the temperature-rise and cooling process were recorded by a thermometer. This experiment of Bi_2Se_3@ZIF-8 was repeated three times for photothermal stability. Herein, the light intensity can remain almost constant as 3 $W \cdot cm^{-2}$ detected by a photoradiometer. Besides, the Ultraviolet-visible-near infrared absorption spectra of Bi_2Se_3@ZIF-8 at 808 nm (0.7 mg/mL) were tested. Detailed calculation methods were showed as follows:

The PTCE (η) can be defined as the fraction of absorbed light energy that is converted to thermal energy, as shown in the following equation:

$$\eta = \frac{hs(T_{max} - T_{surr}) - Q_{Dis}}{I(1 - 10^{-A})} \quad \text{----- Equation S1.}$$

Herein, I is the laser power (3 mW, 1 cm^2); A is the absorbance of aqueous suspension at the wavelength of 808 nm (Figure S10 b); T_{max} and T_{Surr} (30 ºC) are the maximum steady state temperature and the ambient temperature, respectively; h is the heat transfer coefficient and s is the surface area of the container, which are

determined from the following equation:

$$hs = \frac{mc}{\tau_s}$$ ----- **Equation S2.**

m is the mass of the solution (around 0.791 g); c is the specific heat capacity of the solvent (2.5685 J g^{-1} $^{o}C^{-1}$ for MeOH); and τ_s is a time constant, which can be determined in cooling periods from the following equation:

$$t = -\tau_s ln(\theta)$$ ----- **Equation S3.**

θ is a time dependent dimensionless parameter, known as the driving force temperature, defined as follows:

$$\theta = \frac{T - T_{Surr}}{T_{Max} - T_{Surr}}$$ ----- **Equation S4.**

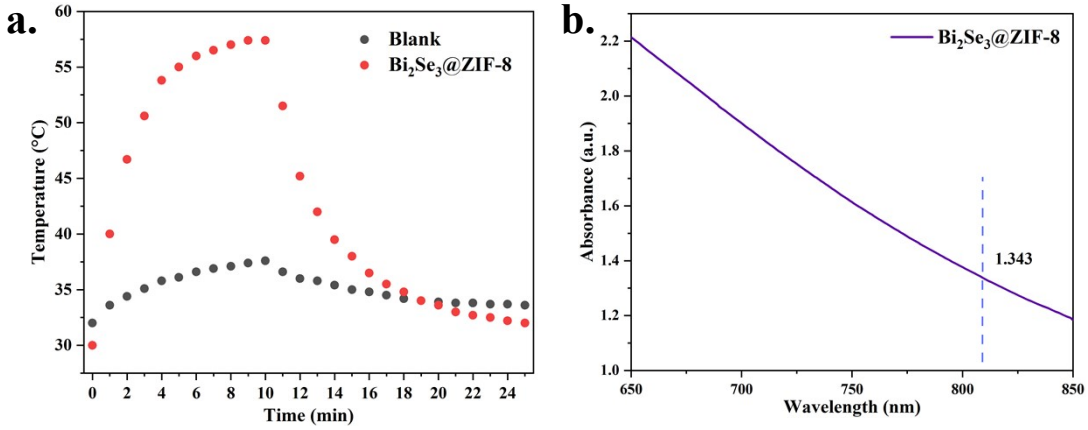

Figure S10. a) Photothermal conversion curves of blank and Bi_2Se_3@ZIF-8 NPs suspensions in MeOH (0.7 mg/mL) under NIR irradiation (808 nm, 3 W·cm^{-2}) for 10 minutes and then switch the laser off. b) The NIR absorption spectra of Bi_2Se_3@ZIF-8 NPs suspensions in MeOH (0.7 mg/mL).

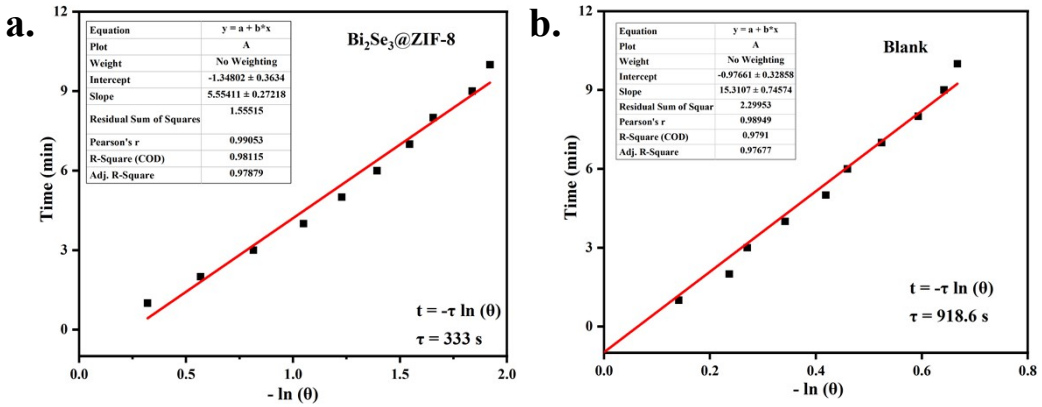

Figure S11. The plots of time versus-ln(θ) from the data recorded during the cooling period (Figure S10 a) of the experiments for Bi_2Se_3@ZIF-8 NPs and blank sample. The slopes can be used to calculate τ_s and PTCE (η).

T_{surr}	T_{max}	Absorbance	τ_s	hs	PTCE (η)
30 °C	61.4 °C	1.343	303	0.0061	6.1%

Table S1. The PTCE (η) of Bi_2Se_3@ZIF-8 NPs calculated by above-mentioned equations.

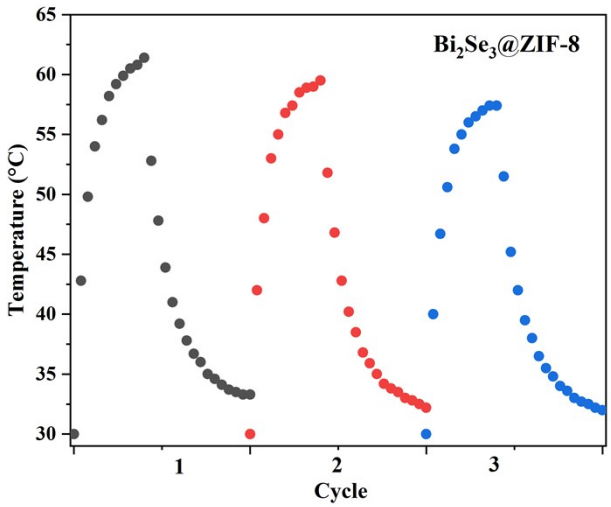

Figure S12. The thermal curve of Bi_2Se_3@ZIF-8 after cyclic irradiation (808 nm, 3 W·cm^{-2}) for three times.

For the purpose of evaluating the photothermal capacity, ZIF-8, Bi_2Se_3 NPs, and Bi_2Se_3@ZIF-8 NPs were placed on a quartz glass sheet under irradiation (808 nm, 0.65 W·cm^{-2}) at ambient atmosphere, respectively. The time-dependent temperature changes were recorded by an IR thermal camera. Meanwhile, a quartz glass without any sample on that was tested under the same condition as blank sample.

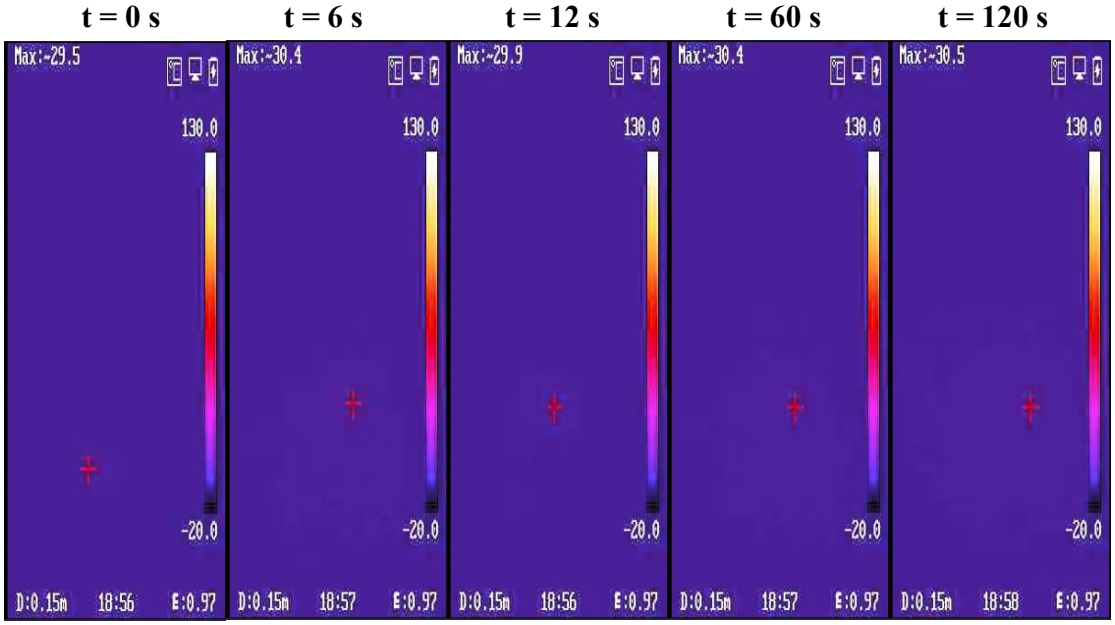

Figure S13. Representative photothermal infrared images of blank at the times of 0, 6, 12, 60, 120 s (0.65 W·cm^{-2}).

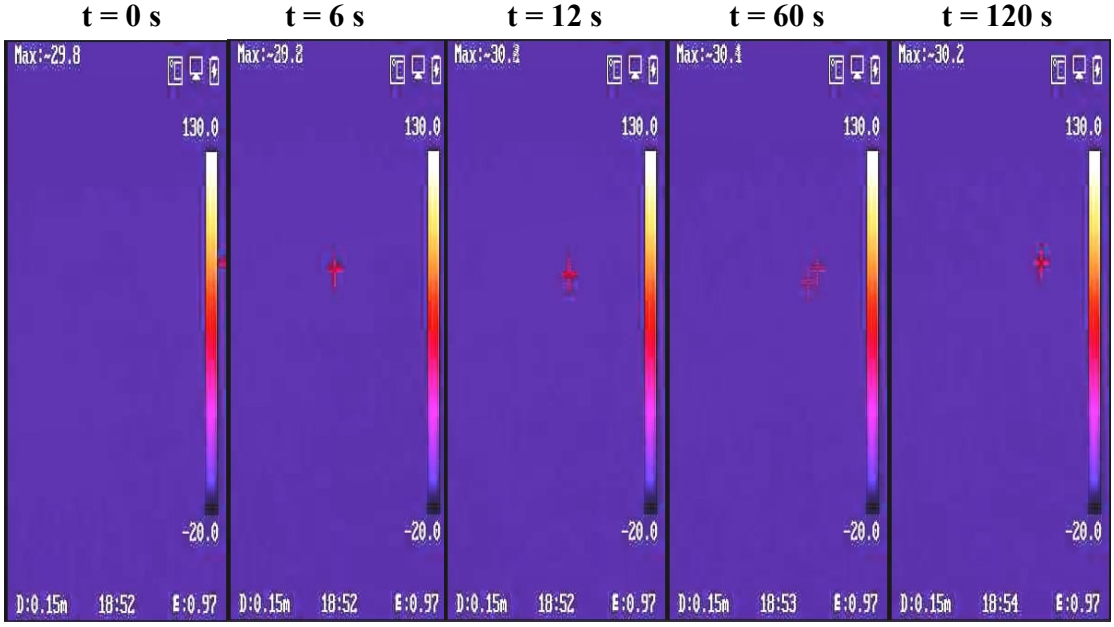

Figure S14. Representative photothermal infrared images of ZIF-8 at the times of 0, 6, 12, 60, 120 s (0.65 W·cm^{-2}).

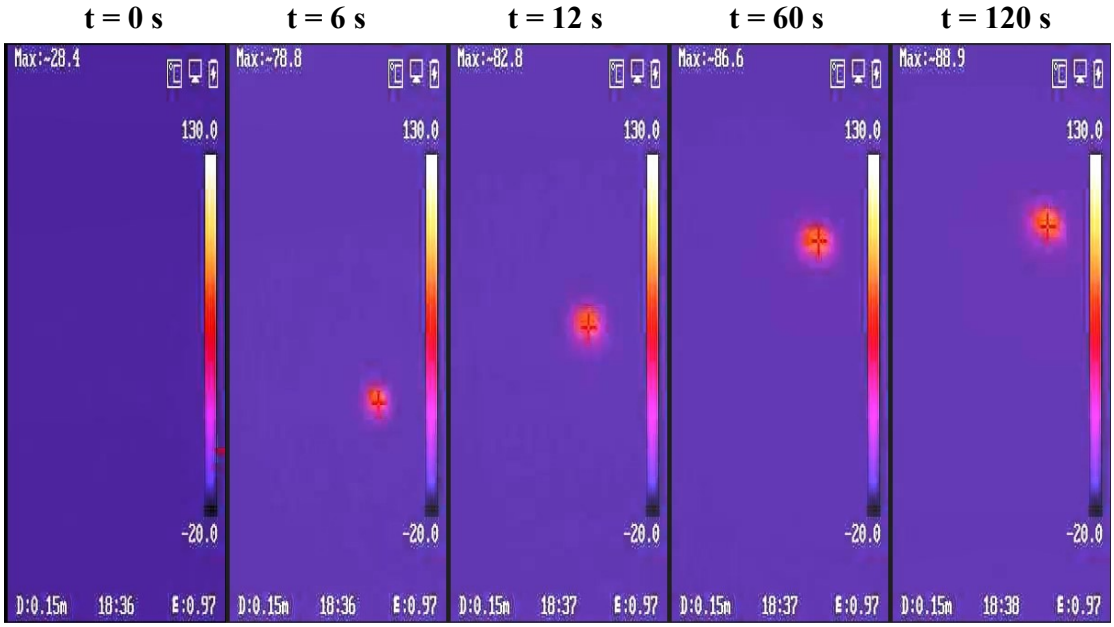

Figure S15. Representative photothermal infrared images of Bi_2Se_3 NPs at the times of 0, 6, 12, 60, 120 s (0.65 W·cm^{-2}).

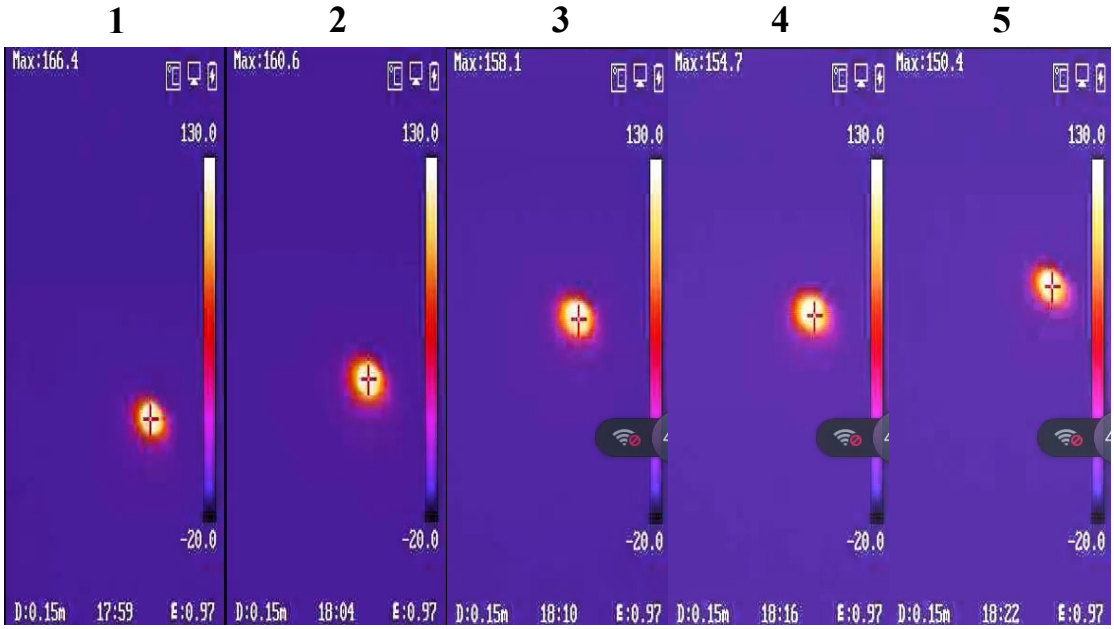

Figure S16. Representative photothermal infrared images of Bi_2Se_3@ZIF-8 NPs in five cycles at the time of 120 s (0.65 W·cm^{-2}).

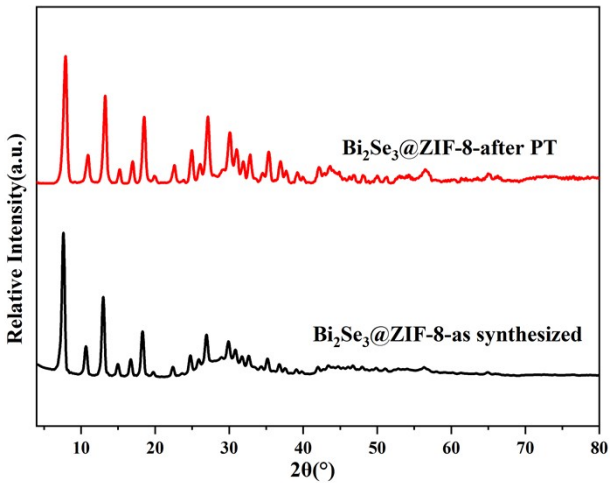

Figure S17. PXRD patterns of Bi_2Se_3@ZIF-8 NPs after multiple irradiation cycles.